Astronomy & Astrophysics

Seismology of Altair with MOST*

Cécile Le Dizès[1,2], Michel Rieutord[1], and Stéphane Charpinet[1]

[1] IRAP, Université de Toulouse, CNRS, UPS, CNES, 14, avenue Édouard Belin, 31400 Toulouse, France
e-mail: Michel.Rieutord@irap.omp.eu, Stephane.Charpinet@irap.omp.eu
[2] Institut Supérieur de l'Aéronautique et de l'Espace (ISAE-SUPAERO), Université de Toulouse, 31400 Toulouse, France
e-mail: cecile.le-dizes@student.isae-supaero.fr

ABSTRACT

Context. Altair is the fastest rotating star at less than 10 parsecs from the Sun. Its precise modelling is a landmark for our understanding of stellar evolution with fast rotation, and all observational constraints are most welcome to better determine the fundamental parameters of this star.

Aims. We wish to improve the seismic spectrum of Altair and confirm the δ-Scuti nature of this star.

Methods. We used the photometric data collected by the Microvariability and Oscillations of STars (MOST) satellite in the form of a series of Fabry images to derive Altair light curves at four epochs, namely in 2007, 2011, 2012, and 2013.

Results. We first confirm the presence of δ-Scuti oscillations in the light curves of Altair. We extend the precision of some eigenfrequencies and add new ones to the spectrum of Altair, which now has 15 detected eigenmodes. The rotation period, which is expected at ~7h46min from models reproducing interferometric data, seems to appear in the 2012 data set, but it still needs confirmation. Finally, Altair modal oscillations show noticeable amplitude variations on a timescale of 10–15 days, which may be the signature of a coupling between oscillations and thermal convection in the layer where the kappa-mechanism is operating.

Conclusions. The Altair oscillation spectrum does not contain a large number of excited eigenmodes, which is similar to the fast rotating star HD220811. This supports the idea that fast rotation hinders the excitation of eigenmodes as already pointed out by theoretical investigations.

Key words. stars: early-type – stars: rotation – stars: variables: δ Scuti

1. Introduction

Altair (α Aquilae, HD187642) is one of the few fast rotating early-type stars in the solar neighbourhood, its distance being 5.13 pc according to HIPPARCOS data (van Leeuwen 2007). As such, it is an ideal target of interferometric observations, which have regularly measured its shape and surface brightness (van Belle et al. 2001; Domiciano de Souza et al. 2005; Monnier et al. 2007). These observations have led to the determination of the centrifugal flattening of Altair which turns out to be close to 22% while its angular velocity at the equator is 74% of the Keplerian one. Such a centrifugal distortion makes the use of two-dimensional models mandatory for a correct interpretation of observational data. Bouchaud et al. (2020) actually performed the first 2D modelling of Altair using ESTER 2D models which include, self-consistently, the 2D structure and the large-scale flows, namely differential rotation and meridional circulation, driven by baroclinicity (Espinosa Lara & Rieutord 2013; Rieutord et al. 2016). Besides demonstrating the young age of Altair (~100 Myrs instead of 1 Gyrs as previously estimated with 1D models e.g., Domiciano de Souza et al. 2005), the work of Bouchaud et al. (2020) shows us that the seismic spectrum of Altair is a key ingredient to further constrain the mass of this star. Indeed, acoustic modes are sensitive to the mean density (Reese et al. 2012; García Hernández et al. 2015), while inter-ferometry, through the measurement of radii, determines the volume of the star.

Hence, the detection of (presumably) acoustic oscillations by Buzasi et al. (2005), in a photometric monitoring of Altair in 1999 by the star tracker of the WISE mission, was a good surprise. This detection meant that Altair is a δ-Scuti star, and actually the brightest one (Buzasi et al. 2005). However, these oscillations were never confirmed. Regarding their importance in the modelling of this star, we looked for new data that would confirm and improve the result of Buzasi et al. (2005). Altair has been quite intensively observed with the Microvariability and Oscillations of STars (MOST) satellite (Walker et al. 2003) in 2007, 2011, 2012, and 2013, but no analysis of these data has been published so far. Since such data have the potential to confirm the previous results and possibly show new frequencies or variations of modes amplitudes, we embarked on a project to process them in order to once again exhibit the seismic spectrum of this fascinating star.

This paper is organised as follows: We first describe the data and the processing we applied to extract the light curves (Sect. 2). We then analyse the light curves and retrieve the oscillation spectra at the various epoch of the data (Sect. 3). A discussion and preliminary conclusions end the paper.

2. Observations and data reduction

Altair was observed in four sequences by the MOST satellite, which run around the Earth at a mean altitude of 830 km with an orbital period of 6084.9 s, corresponding to a frequency of

---

* This work is based on data from the MOST satellite, a Canadian Space Agency mission, jointly operated by Dynacon Inc., the University of Toronto Institute for Aerospace Studies and the University of British Columbia, with the assistance of the University of Vienna.
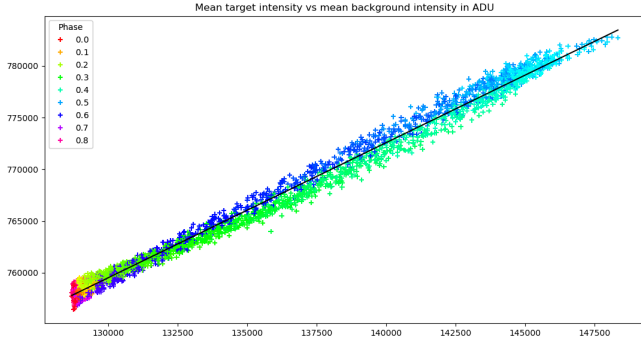
Fig. 1. Correlation between target and background pixels. Colours indicate the orbital phase of MOST.

Fig. 2. Effects of the different reduction steps on the magnitude amplitude for the 2011 set. *Top*: original data. *Middle*: data after the decorrelation step. *Bottom*: data after the decorrelation and removal of the mean orbit. Colours indicate the orbital phase of MOST.

14.199 c/d (Walker et al. 2003). The characteristics of the time series are summarised in Table A.1.

Data were downloaded from the Canadian Astronomy Data Centre. They are available as a series of Fabry images, from which we derived light curves. In Appendix A, we provide some details on the first steps of this processing, but the main challenge of this data reduction is the clean suppression of stray light, which comes from the illuminated side of the Earth or from moonshine.

The technique we used is inspired by the one developed by Huber & Reegen (2008) and is based on calculating correlations of mean target and background flux. Since stray light is variable over timescales of approximately a day, the correlation was calculated using the mean background and target intensity in a moving window of 1 day rather than using the whole light curve. An example of a linear correlation between target and background pixels is shown for the 2011 data set in Fig. 1.

This method assumes that the influence of stray light is the same for target and background pixels, and that the background pixel intensity is not influenced by the star light.

The correction of the correlation was made by measuring the variations δm between the real target magnitude and the one given by the linear trend each time. Hence,

$$\delta m(t) = -\frac{5}{2 \ln 10} \ln \left[\frac{I_{\text{tar,real}}(t)}{I_{\text{tar,correl}}(t)} \right], \tag{1}$$

where $I_{\text{tar,real}}(t)$ is the mean intensity of the target pixels at time t, and

$$I_{\text{tar,correl}}(t) = a I_{\text{bck,real}} + b,$$

where $I_{\text{bck,real}}(t)$ is the mean intensity of the background pixels at time t, and a, b are the coefficients given by the linear regression.

As discussed in Huber & Reegen (2008), our procedure is a simplified version of the algorithm of Reegen et al. (2006), which searches for the background pixels that best correlate with each target pixel. In the procedure of Reegen et al. (2006), the background flux is removed from the target pixel intensity and the procedure is repeated on the next target pixel until all stray light contributions have been reduced to an acceptable level.

Such a procedure is able to remove a non-uniform stray light pattern, but it is quite demanding in computation time. We did not implement this type of processing since, in the end, the simple algorithm described previously, with some additional processing detailed below, satisfactorily removed the periodic signal coming from stray light.

Hence, to further remove the effects of the orbital period at a frequency of 14.199 c/d, we used a moving window of 28
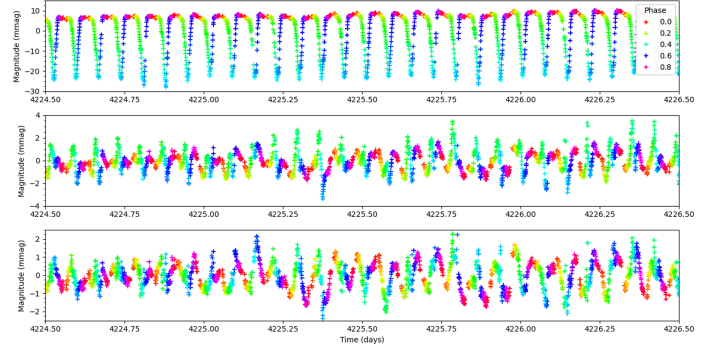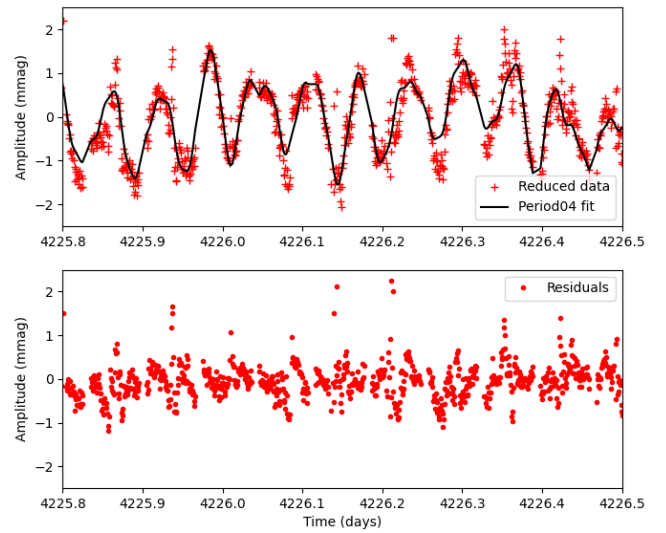

Fig. 3. Amplitude (in mmag) versus time (in days) for a portion of the 2011 light curve. *Top*: reduced data with the solid line showing the fit given by Period04. *Bottom*: residuals after subtraction of the fit.

periods (~2 d) to create a mean light curve folded at the MOST orbital period and removed this mean light curve from the data. This step effectively suppressed the harmonics of the orbital frequency from the final power spectra.

To illustrate this processing, we show in Fig. 2 the evolution of the light curve at each step using a subset of the 2011 data. The final light curve, a glimpse of which is shown in Fig. 3, typically gives amplitude fluctuations of ±2 mmag. This is similar to those observed by Buzasi et al. (2005) and also quite similar to those of Rasalhague (α Ophiuchi), another fast rotating A-type star with δ-Scuti oscillations (Monnier et al. 2010).

Figure 4 further shows the role of the processing steps on the power spectra of the light curves using Period04 (Lenz & Breger 2005). The orbital frequency at 14.199 c/d clearly shows up in the unprocessed data, as well as in the decorrelated data (at a lower level of course). We also notice secondary peaks separated from the orbital frequency by $\delta\nu = 1$ c/d or multiples of it, namely associated with Earth's rotation. Figure 4 clearly shows that the removal of the mean orbit signal and global decorrelation quite nicely suppresses most of the systematics coming from the orbital motion of MOST.
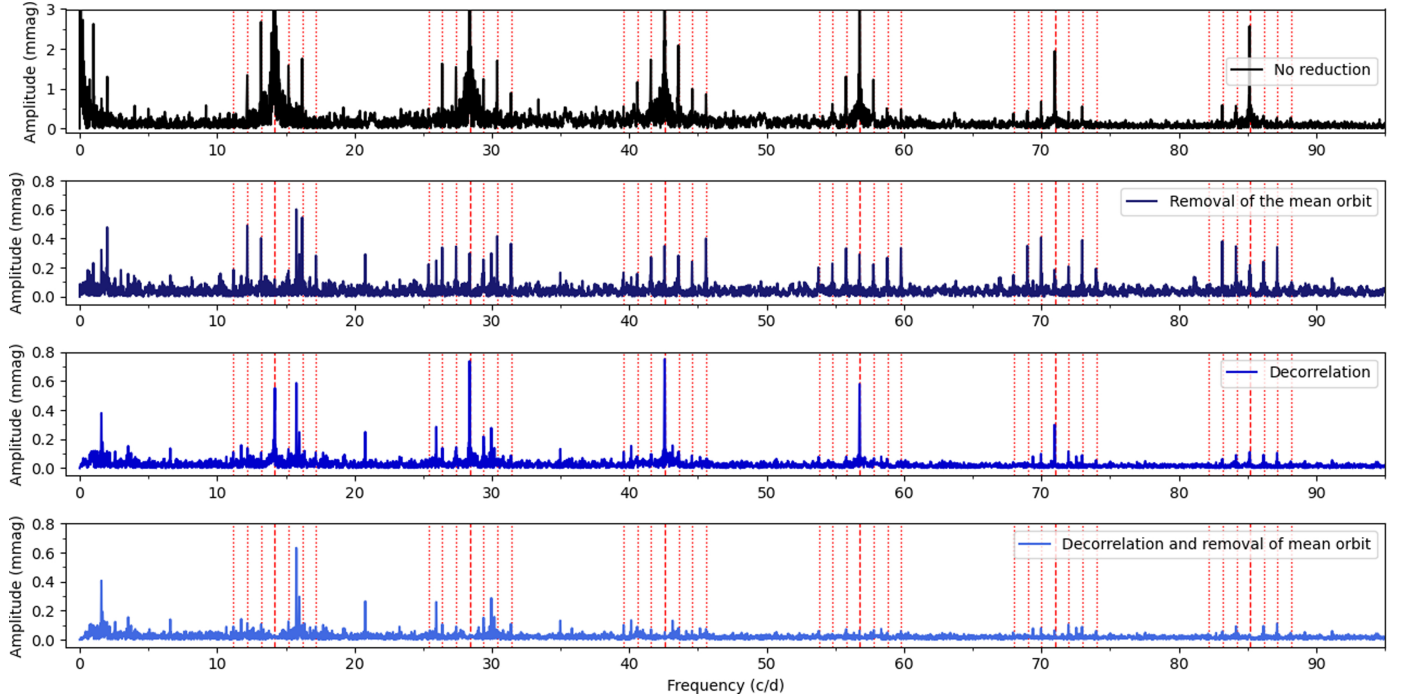
Fig. 4. Effects of different reduction techniques on the amplitude spectrum for the 2012 set. The dashed red lines show the orbital frequency and its harmonics. The red dotted lines are evenly spaced 1 c/d apart from one another.

Table 1. Comparison of various software (`Period04`, FELIX, PYPE) at determining the frequency and amplitude of two modes with different difficulty.

		2011			2012		
		`Period04`	FELIX	PYPE	`Period04`	FELIX	PYPE
Mode 1	F	15.7677 ± 46	15.7657 ± 37	15.7812 ± 16	15.7685 ± 3	15.7686 ± 4	15.7689 ± 1
	A	585 ± 12	564 ± 15	662 ± 11	590 ± 19	583 ± 15	583 ± 7
Mode 2	F	20.7898 ± 60	20.7832 ± 81	20.7898 ± 35	20.7865 ± 6	20.7866 ± 9	20.7863 ± 4
	A	241 ± 10	246 ± 14	245 ± 7	262 ± 8	262 ± 14	262 ± 6

Notes. The 2011 data are short (4 days long) and thus less resolved than the 2012 data (33 days long). The 15.77 c/d is close to two other frequencies, while the 20.79 c/d mode is isolated. Frequencies (F) are in c/d, their uncertainties are in 10^{-4} c/d, while amplitudes (A) are in ppm as their uncertainties.

3. Analysis

3.1. Algorithm – Validation

After the foregoing extraction of the light curves from the raw data, we proceeded with the derivation of the frequencies and amplitude of the modes. For that purpose, we used several types of software that are all based on the same classical method, involving computing the Lomb-Scargle periodogram, pre-whitening the signal, and adjusting a combination of sinusoidal signal as

$$I(t) = \sum_{n=1}^{N} A_n \sin(2\pi\nu_n t + \phi_n) \tag{2}$$

to the data through non-linear least-square optimisation. We used `Period04` (Lenz & Breger 2005), FELIX (Charpinet et al. 2010; Zong et al. 2016), and PYPE, which is a python software specially built for this work from python libraries (Astropy 4.2 for the Lomb-Scargle periodogram and Scipy for the optimisation). These types of software differ from one another basically from their evaluation of uncertainties.

Period04 uses Monte-Carlo simulations, FELIX uses formulae from Montgomery & O'Donoghue (1999), while PYPE is based on the bootstrap method. Comparison of the results from these three types of software is useful to appreciate the influence of the numerical procedure on the results. Basically, the programmes usually agree, especially when the quality of the data increases, not surprisingly. We show in Table 1 the results for two modes using the three programmes. This illustrates that amplitudes of the main mode are badly determined with the 2011 data due to their short length (4 days), mostly because of the mixture of this mode with its neighbouring one at 15.98 c/d.

3.2. Error bars, noise

Before presenting the results, we first discuss their sources of uncertainties. As written above, we assume that the flux variations of Altair are due to excited eigenmodes in the small amplitude regime and they can be represented by the series (2). The amplitudes A_n, the frequencies ν_n, or the phase ϕ_n are the parameters of the model whose uncertainties are to be evaluated. These uncertainties basically have three sources: (i)
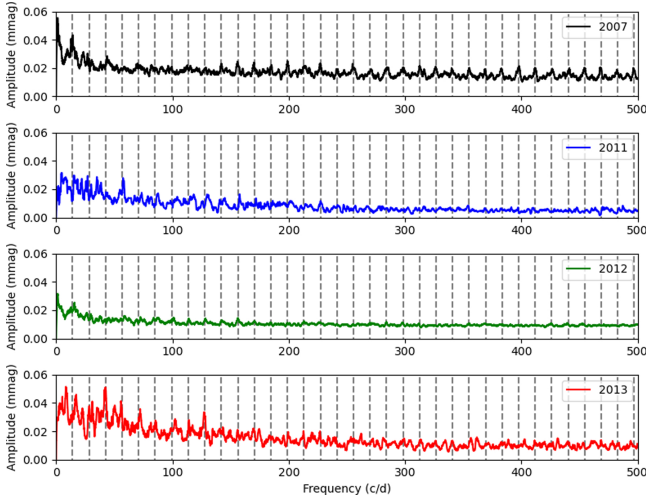
Fig. 5. Noise spectrum calculated for each data set with the residuals of pre-whitened light curves with 16 frequencies.

residual stray light (ii), random noise (iii), and time sampling of the signal.

As far as residual stray light is concerned, it is characterized by its frequencies that are typically of the form $F_{nm} = n f_{orb} \pm m f_{day}$, which we detected for $0 \leq n \leq 7$ and $0 \leq m \leq 4$. These spectral lines prevented us from detecting or correctly measuring any signal in frequency bands such as $[F_{nm} - \Delta f, F_{nm} + \Delta f]$, where Δf is the frequency resolution of the window data set. As a consequence, Altair's frequency oscillation at 28.40 c/d $\simeq 2 f_{orb}$ detected by Buzasi et al. (2005) was just screened by the stray light signal (and the time window which includes this harmonic). The same pollution affects the oscillation at 16.18 c/d close to the frequency $f_{orb} + 2 f_{day}$.

Next, the influence of intrinsic noise was evaluated by either the bootstrap method (PYPE), Montgomery & O'Donoghue (1999) analysis (FELIX), or Monte-Carlo simulations (Period04). We note that sometimes Monte-Carlo simulations of Period04 do not give realistic results, especially on noisy data. By pre-whitening the signal until the standard deviation of the remaining light curve was approximately constant, we got an idea of the random noise. The amplitudes of this noise for the four data set at hand are:

2007: 1456 ppm, 2011: 224 ppm,
2012: 414 ppm, 2013: 374 ppm

The 2007 data set is obviously the noisiest due to large pointing errors, but its length (~20 days) somehow compensates for this. The best data set is the one from 2012 because of its length and moderate noise. This is also illustrated in Fig. 5 where we plotted the noise spectrum for the four data sets. Clearly 2007 appears very much polluted by stray light, while 2012 appears to be the best series. We note that 2011 and 2013 have most of their noise in the [0, 50]c/d range, which is also the range of interest, unfortunately.

4. Results

4.1. Altair's oscillation spectrum

Figure 4 has already shown a view of the Altair oscillation spectrum with 2012 data. However, as discussed below, the modes amplitude varies with time. We therefore extracted, from each data set, the most significant frequencies along with their amplitude and they are represented in a periodogram-like plot in

Fig. 6. From this spectrum, we extracted a list of modes, whose detection we consider as the most reliable. Their frequencies and amplitudes are gathered in Table 2. Most of them appear in several data sets, making their detection quite robust.

The first impression one gets looking at Altair's spectrum is that it is rather sparse if we compare it to the well-studied (Chen et al. 2016; Balona 2014) δ-Scuti HD50844 observed by CoRoT (Poretti et al. 2009). Of course, HD50844 is near the TAMS and Altair is close to the ZAMS (Bouchaud et al. 2020). In addition, Altair's rotation period is eight times shorter than that of HD50844. Altair's oscillation spectrum better compares with that of stars picked out by Bedding et al. (2020). These stars are young with intermediate mass showing δ-Scuti oscillations just as Altair. But unlike them, Altair does not show modes with frequencies above 40 c/d, nor a clear regular spacing of frequencies. Actually we might note an approximately recurrent spacing of ~2.5 d^{-1} with frequencies f_6, f_{10}, f_{11}, f_{12}, f_{13}, and f_{15}, as already pointed out in Bouchaud et al. (2020).

Another regular spacing, ~0.907 c/d, may also be noticed within the low frequencies f_2, f_3, f_4, f_5. Monnier et al. (2010) observed a similar pattern for two sets of modes in the oscillation spectrum of α Ophiuchi, with a spacing of ~1.71 c/d and ~1.74 c/d, respectively. These authors interpreted these sets of modes as the possible signature of equatorial Kelvin waves. This is an appealing interpretation, but in our case we shall wait for the spectroscopic data that are expected shortly before deciding on the meaning of these quasi-regular patterns at low frequency (Rieutord et al., in prep.).

We also observed something similar to a triplet of frequencies f_6, f_7, f_8 around $\nu = 16$ c/d with the most powerful peak of Altair's spectrum at 15.7679 c/d. The frequency spacing of 0.2 c/d of course does not correspond to a rotational splitting which would be much larger. A search in the theoretical predictions based on the 2D model of Altair computed in Bouchaud et al. (2020) does not show conspicuous evidence of modes that could be identified with the detected frequencies. However, the theoretical modelling is not ripe yet, lacking the selection criterion of excited modes.

4.2. HD220811: Potential sister of Altair

Interestingly, Altair's spectrum shows some similarities with that of HD220811 taken from the list of Bedding et al. (2020). As shown in Fig. 7, the two stars show their main excited modes in the range of 15–40 c/d and coincidentally both show a strongly excited mode at $f \sim 15.9$ c/d. Not much is known about HD220811: It is a double star with a tiny separation of 0.4″. The Transiting Exoplanet Survey Satellite (TESS) input catalogue says its effective temperature is 7527 K, which is close to the average Altair's effective temperature of 7550 K (Erspamer & North 2003). Its $V \sin i \sim 270$ km s^{-1}, according to Bedding et al. (2020), is compatible with the 313 km s^{-1} equatorial velocity of Altair (Bouchaud et al. 2020). The TESS input catalogue also mentions a HIPPARCOS parallax of 8.57 mas and a visual magnitude of 6.91. Using Altair's parallax 194.44 mas and visual magnitude of 0.76, we deduce that the apparent luminosity of HD220811 is slightly larger than that of Altair, namely $L_{HD220811} \simeq 1.8 \, L_{Altair}$. Since this luminosity is only the apparent one, which depends on the inclination of the rotation axis, the two stars may well be very similar.

The probable similarity of Altair and HD220811 as far as their oscillation spectrum and spectral type are concerned, together with their very fast rotation ($V_{eq} \sim 300$ km s^{-1}), may illustrate the result of Reese et al. (2017) that fast rotation
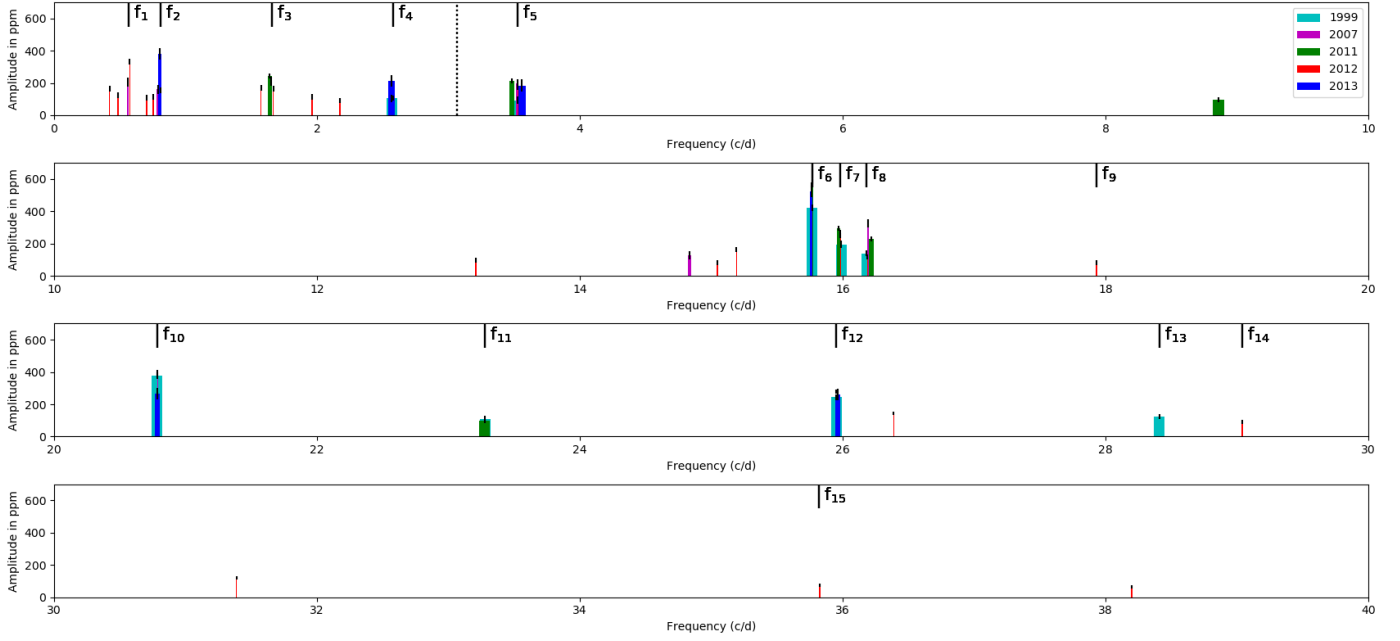
Fig. 6. Idealised amplitude spectrum of Altair derived from the analysis of the four data sets of MOST. The width of the bars shows the frequency uncertainty, while the little vertical bars over the thick previous bars show the amplitude uncertainty. Frequency labels refer to Table 2. Some unlabelled frequencies have been left and just await confirmation from future observations. The dotted vertical line indicates the expected frequency of Altair's rotation.

Table 2. Oscillation frequencies that have been detected at an S/N above 4.

	Frequency (c/d)	$\langle A \rangle$ (ppm)	Years of detection
f_1	0.57 [*]	270	2007, 2012
f_2	0.81 [*]	160	2007, 2012
f_3	1.66 [*]	200	2007, 2012
f_4	2.58	100	1999, 2012, 2013
f_5	3.527	150	1999, 2007, 2012, 2013
f_6	15.7679	520	1999 → 2013
f_7	15.983	260	1999, 2007, 2012
f_8	16.180	140	1999
f_9	17.93 [*]	80	2012
f_{10}	20.7865	330	1999 → 2013
f_{11}	23.28	110	1999, 2007
f_{12}	25.952	220	1999 → 2013
f_{13}	28.408	120	1999
f_{14}	29.04 [*]	100	2007, 2012
f_{15}	35.82 [*]	80	2007, 2012

Notes. The six starred frequencies are new and complete those detected by Buzasi et al. (2005). Uncertainties on frequencies are typically 0.02 c/d or better. As amplitudes vary in time (see Sect. 4.4), an average value is given.

reduces the number of excited modes in a star. The parallel study of these two stars, and others with the same features, will be very useful to better appreciate all the effects of rotation.

4.3. Rotation

From interferometric and spectroscopic data, Bouchaud et al. (2020) derived the angular velocity of Altair which corresponds to $\nu_{\rm rot} = 3.08 \pm 0.03$ c/d. In fact, from the Bouchaud et al. (2020)

model of Altair, we have an idea of the surface differential rotation of this star. It is shown in Fig. 8 along with its uncertainty. A flux pattern at the surface of Altair may therefore show up at a frequency in between 2.9 and 3.16 c/d. A close-up of the spectrum in this range (see Fig. 9) shows a signal at 2.99 c/d in the 2012 data set, which may be a signature of a such a flux pattern. Since Altair is known to be magnetically active (Robrade & Schmitt 2009), flux modulation by some magnetic feature at its surface is not impossible. However, this possible detection of rotation needs to be confirmed.

4.4. Time variability

The data sets collected by MOST over the years offer the possibility to investigate the time variation of the modes amplitude. However, the determination of the amplitude of a mode depends on the determination of its frequency. The length of the light curves and the time windows are unfortunately not constant from one set to another. Mode frequencies are therefore more or less well determined according to the data set at hand. However, for the modes listed in Table 2, frequencies can be considered as constant within their error bar. Thus, we shall assume their constancy in time. We therefore determined the best frequency of the main modes using all data and projected the desired subset of the light curve on the simple Fourier basis (e.g., Eq. (2)) using least-squares to obtain the time evolution of amplitudes over the years.

A first view of these variations of the main modes over the years is shown in Fig. 10. The most prominent mode at $f = 15.7679$ c/d shows a rather important growth (a factor of 1.5) between 1999 and 2007. With the origin of these variations being numerous (see Guzik et al. 2016 for a rather exhaustive list), a hint may be given by the timescales shown by these fluctuations. Figure 10 shows that years should be considered, but phenomena such as convection may impose much shorter timescales and suggest for one to inspect variations over days. To this end, we
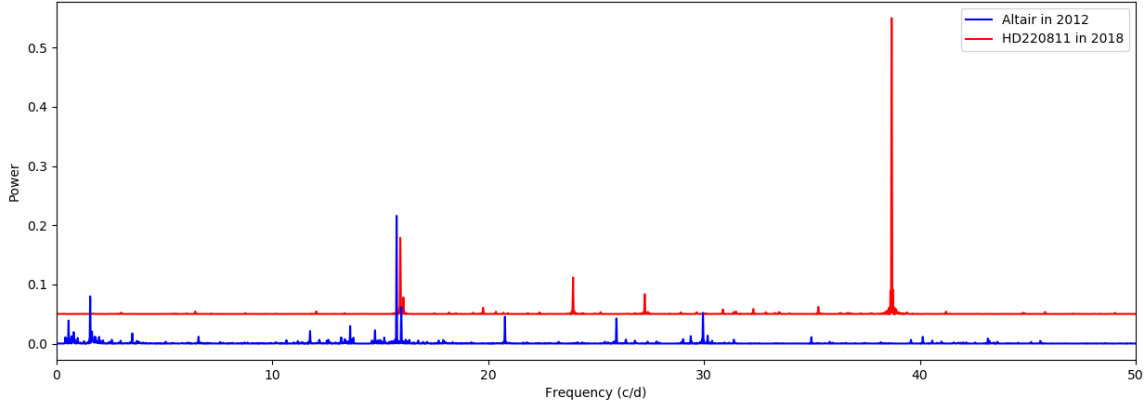
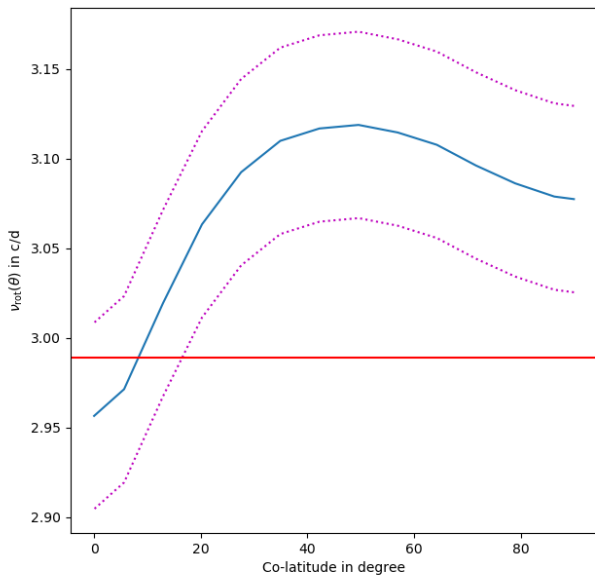**Fig. 7.** Superposition of Altair's and HD220811 spectra.

Fig. 8. Surface differential of Altair from the 2D model of Bouchaud et al. (2020) expressed by a frequency in c/d as a function of co-latitude (solid blue line). The dotted lines show the 2-sigma uncertainty of the model parameter, while the horizontal red line shows the frequency 2.99 c/d, which shows up in the 2012 data in Fig. 9.
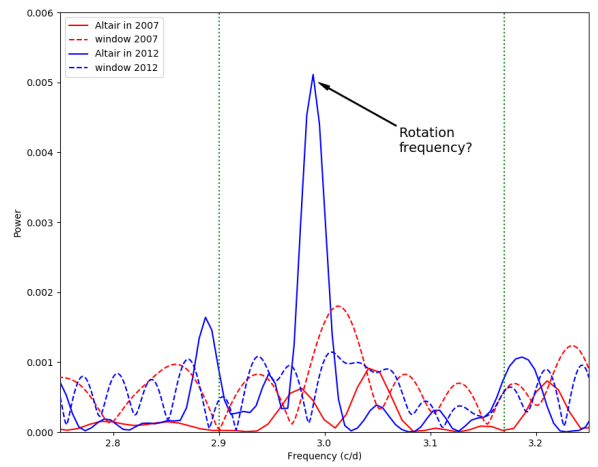

Fig. 9. Close-up of the spectrum near the expected rotation frequency. The two dotted vertical lines show the 2-sigma interval where the rotation could be found including the effects of surface differential rotation.

Fig. 10. Time variability of the amplitudes (in ppm) of the six dominant modes with uncertainties.

concentrated on the 2012 data set, which is certainly the most appropriate with its 33 days length and its rather low noise. We first carried out a time-frequency analysis with a one-day time step and a 3.3 days interval. The result is shown in Fig. 11.

We clearly see amplitude oscillations near 15.8 c/d due to the two beating modes at 15.7679 and 15.983 c/d, but an evolving trend is also visible along the time interval. This evolution is better seen if we split the time interval into disjoint windows of 3.3 days. Shorter windows do not provide more information and they are influenced by noise or secondary window peaks too much. This is why we do not show the amplitude variation of the f_7-mode, which is too close to the main f_6-mode at $f = 15.7679$ c/d. Hence, the amplitude variations of f_6 also include those of f_7. Figure 12 shows the amplitude variations of the five most prominent modes. This figure suggests an amplitude variation on a timescale of 15 days for the main mode at f_6 and for the low amplitude mode at f_{11}, whose variations are anti-correlated with those of f_6. The amplitude of the beating effect between f_6 and f_7 is also shown in Fig. 12 (black dashed line). For that, we generated a light curve where the two
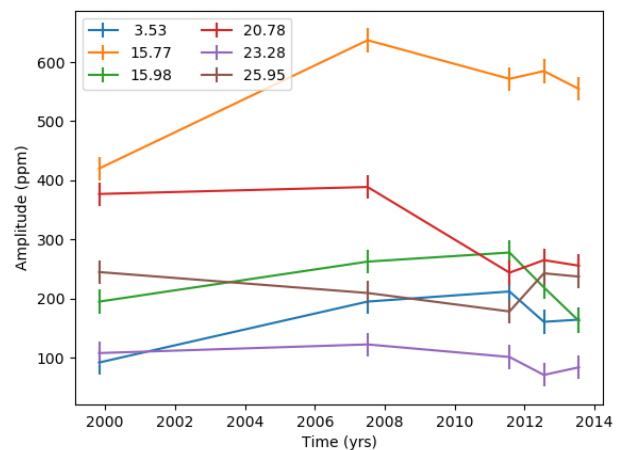
modes f_6 and f_7 have a constant amplitude, and we processed this artificial light curve in a similar way as the real one. We can clearly see that the beating effect produces amplitude variations that are much smaller than those observed on f_6. Mode f_{10} also seems to show, mildly, an amplitude evolution on a
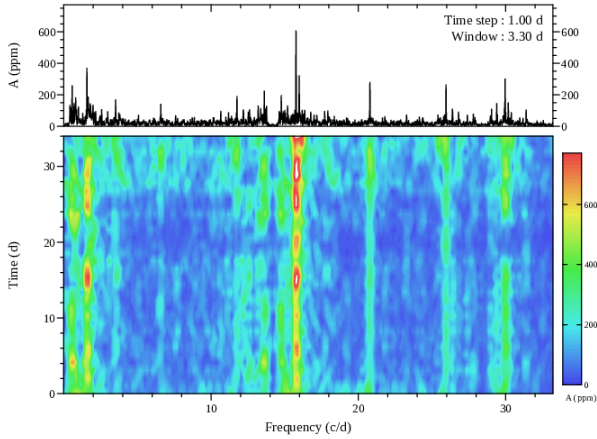
Fig. 11. Time-frequency diagram for the 2012 observation set. Time starts at JD-JD2000 = 4576.093.
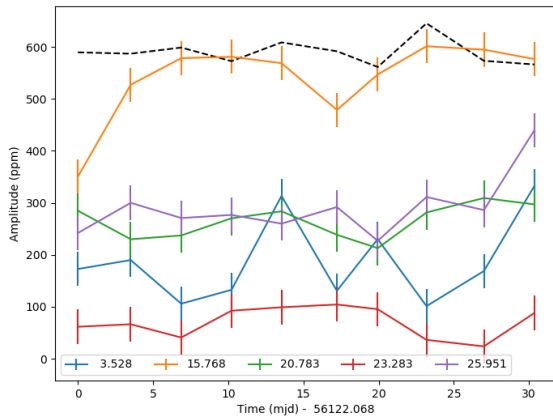

Fig. 12. Time variability of the amplitudes (in ppm) of the five dominant modes with uncertainties during the 2012 observations. The black dashed line shows the amplitude variations of the $f_6 = 15.768$-mode if they were only due to the beats with the $f_7 = 15.983$-mode.

15-day timescale. The low-frequency mode at $f_5 = 3.527$ c/d seems to show an amplitude modulation on a 10-day timescale (e.g., Fig. 11), while the mode at f_{12} also shows amplitude variations, but on a timescale similar to the window sampling, which hinders any conclusion being made. The driving of δ-Scuti oscillations is classically attributed to the κ-mechanism associated with the opacity bump generated by the partial second ionisation of helium around 50 000 K (Baglin et al. 1973; Balona et al. 2015). However, such an opacity bump also destabilises a whole layer of the star where thermal convection arises. This convection occurs at high Reynolds numbers and thus excites a wide range of time and length scales. Using Bouchaud et al. (2020) Altair's model, we found that timescales of 10 or 15 days are well within the possible timescales of convection in the κ-exciting layer. This coincidence may not be just by chance and further work is needed to explain the way oscillations may be modulated on this timescale.

5. Conclusions

Buzasi et al. (2005) discovered that Altair is the brightest δ-Scuti of the sky, and we confirm this. The oscillation spectrum of Altair now includes six new frequencies and we extend the range of frequencies from 0.57 c/d to 35.82 c/d. The MOST observations of Altair, distributed over several years, allowed us to

bring the variations of the mode amplitudes to light. The time frequency analysis of the 2012 data set, which spans 33 days, showed characteristic timescales of ~10 to 15 days, which can be imposed by the convective layer associated with the opacity bump of helium second ionisation. Since this opacity bump is also known to drive oscillations in δ-Scuti stars, a good modelling of the coupling of thermal convection with oscillations, in the spirit of Gastine & Dintrans (2011), would offer an opportunity to use these amplitude variations to constrain the physics of the stars in this layer.

The number of modes excited at a detectable amplitude in Altair is still rather modest (15 if we were to gather all data). HD220811, which is quite similar to Altair as far as T_{eff} and V$\sin i$ are concerned, also shows a similar number of frequencies. This point is reminiscent of the theoretical (preliminary) result of Reese et al. (2017), which shows that as the rotation rate increases, mode excitation is less and less efficient. In other words, rotation tends to stabilise modes otherwise destabilised by the κ-mechanism.

Finally, we may have detected the signature of Altair's rotation as a spectral peak popping up at 2.99 c/d, which is fully compatible with present models of Altair (Bouchaud et al. 2020). However, this detection still demands confirmation as it is only visible in the 2012 light curve.

The foregoing results encourage us to obtain more data on the seismology of Altair. This will be the case with the shortly awaited analysis of line profile variations that allow us to detect eigenmodes with a high azimuthal wavenumber propagating in longitude (Rieutord et al., in prep.). With a larger set of eigenfrequencies, we will be in a better position to bring new constraints on the fundamental parameters of Altair, our nearest fast rotating star.

References

Baglin, A., Breger, M., Chevalier, C., et al. 1973, A&A, 23, 221
Balona, L. A. 2014, MNRAS, 439, 3453
Balona, L. A., Daszyńska-Daszkiewicz, J., & Pamyatnykh, A. A. 2015, MNRAS, 452, 3073
Bedding, T. R., Murphy, S. J., Hey, D. R., et al. 2020, Nature, 581, 147
Bouchaud, K., Domiciano de Souza, A., Rieutord, M., Reese, D. R., & Kervella, P. 2020, A&A, 633, A78
Buzasi, D. L., Bruntt, H., Bedding, T. R., et al. 2005, ApJ, 619, 1072
Charpinet, S., Green, E. M., Baglin, A., et al. 2010, A&A, 516, L6
Chen, X. H., Li, Y., Lai, X. J., & Wu, T. 2016, A&A, 593, A69
Domiciano de Souza, A., Kervella, P., Jankov, S., et al. 2005, A&A, 442, 567
Erspamer, D., & North, P. 2003, A&A, 398, 1121
Espinosa Lara, F., & Rieutord, M. 2013, A&A, 552, A35
García Hernández, A., Martín-Ruiz, S., Monteiro, M. J. P. F. G., et al. 2015, ApJ, 811, L29
Gastine, T., & Dintrans, B. 2011, A&A, 528, A6
Guzik, J. A., Kosak, K., Bradley, P. A., & Jackiewicz, J. 2016, IAU Focus Meeting, 29B, 560
Huber, D., & Reegen, P. 2008, Commun. Asteroseismol., 152, 77
Lenz, P., & Breger, M. 2005, Commun. Asteroseismol., 146, 53
Monnier, J. D., Zhao, M., Pedretti, E., et al. 2007, Science, 317, 342
Monnier, J. D., Townsend, R. H. D., Che, X., et al. 2010, ApJ, 725, 1192
Montgomery, M. H., & O'Donoghue, D. 1999, Delta Scuti Star Newsl., 13, 28
Poretti, E., Michel, E., Garrido, R., et al. 2009, A&A, 506, 85
Reegen, P., Kallinger, T., Frast, D., et al. 2006, MNRAS, 367, 1417

Reese, D. R., Marques, J. P., Goupil, M. J., Thompson, M. J., & Deheuvels, S. 2012, A&A, 539, A63

Reese, D. R., Dupret, M. A., & Rieutord, M. 2017, Eur. Phys. J. Web Conf., 160, 02007

Rieutord, M., Espinosa Lara, F., & Putigny, B. 2016, J. Comp. Phys., 318, 277

Robrade, J., & Schmitt, J. H. M. M. 2009, A&A, 497, 511

van Belle, G. T., Ciardi, D. R., Thompson, R. R., Akeson, R. L., & Lada, E. A. 2001, ApJ, 559, 1155

van Leeuwen, F. 2007, A&A, 474, 653

Walker, G., Matthews, J., Kuschnig, R., et al. 2003, PASP, 115, 1023

Zong, W., Charpinet, S., & Vauclair, G. 2016, A&A, 594, A46

Appendix A: Pre-processing of MOST data

Table A.1. Summary of characteristics of data sets.

	2007	2011	2012	2013
From	25 June	26 July	12 July	17 July
JD−JD2000	2732.18	4223.51	4576.09	4946.06
to	15 July	30 July	28 August	25 July
JD−JD2000	2752.34	4227.50	4609.49	4954.04
Duration (d)	20.166	3.992	33.398	7.986
Gaps	/	/	1 d	3.5 d
N_0	37,729	4,834	23,555	4,849
N	30,544	4,578	21,701	4,658
Percentage of pointing errors	19.15%	5.30%	4.79%	3.94%

Notes. We note that N_0 is the number of pictures in the initial series, while N is the number of pictures left after the removal of the problematic ones.

Data from MOST come as a series of Fabry images where the star light is projected onto the CCD by a Fabry microlens as an annulus covering about 450 pixels as shown in Fig. A.1. We reduced the data using different techniques inspired by Reegen et al. (2006).

The first step was to remove discontinuities that appear in the time series of Altair. These discontinuities are also present in the time series of the guide stars (Fig. A.2). By analysing the headers in the fits file, we believe that these discontinuities are due to a change in the acquisition parameters of the telescope to improve the contrast. We removed these discontinuities by adding the appropriate constant.

The Attitude Control System gives a set of xy-errors for each image. These error values indicate whether or not the target is
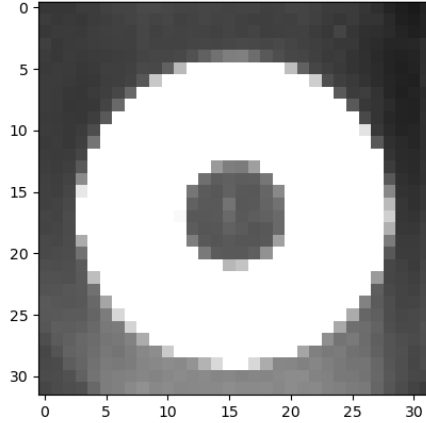

Fig. A.1. Example of a Fabry image obtained from observations of Altair with the Fabry lens from the 2012 data set. We note the non-uniform background due to stray light.
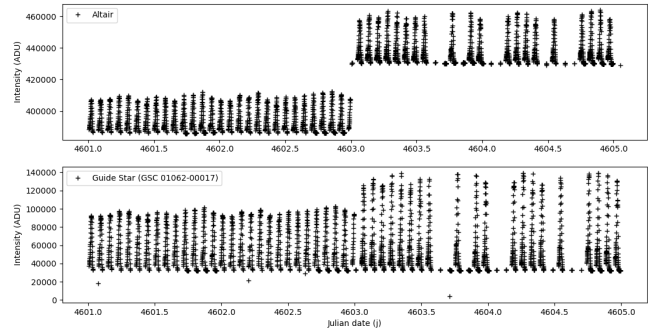

Fig. A.2. Mean intensity versus time (2012 data set) for Altair (top) and the guide star (bottom).

inside the nominal Fabry lens area. When the x-errors or y-errors cross the limits of the interval [−25.8, 25.8] (in arcsec) during the integration time, the maximum value is returned. We rejected all images with out-of-range xy-errors and 3σ outliers.

The effects of removing bad data are shown in Table A.1. For the 2007 data, this sorting removes ∼19% of the data points. This rather high rate of bad data was related to the pointing precision of MOST, which was improved later, and does not affect data from 2011, 2012, and 2013.

The last step needed to derive the light curves of Altair was to decorrelate Altair's light from stray light. This important step is described in the main text.